



Nanochitosan Reinforced Polyvinyl Alcohol/Cashew Gum Bio-blend Nanocomposites: Promising Materials for Future Frontiers

K. Meera¹ · K. Arun¹ · M. T. Ramesan¹

Accepted: 3 May 2023 / Published online: 16 May 2023

© The Author(s), under exclusive licence to Springer Science+Business Media, LLC, part of Springer Nature 2023

Abstract

Herein, biopolymer nanocomposite films were prepared from the blend of two polymers, polyvinyl alcohol (PVA) and cashew gum (CG), incorporated with various concentrations of nanochitosan (nCS) via the green solution casting method. The effects of nCS on the structural, morphological, mechanical, thermal and electrical/dielectric characteristics of the PVA/CG blend have been investigated and discussed. The major absorption peaks of PVA and CG were revealed by the Fourier transform infrared study, and their positions slightly changed with the insertion of nCS. X-ray diffraction results revealed that the crystallinity degree of the nanocomposite samples increased with increasing nCS content. The consistent distribution of chitosan nanofillers in the blend network was visible in the scanning electron microscopy images. Differential scanning calorimetry and thermogravimetric analysis showed that increasing the nanofiller loading into the PVA/CG increased the glass transition temperature and thermal stability. The electrical impedance measurements showed that the nanofiller loading increases the electrical conductivity and dielectric properties. The AC conductivity of PVA/CG/7wt% nCS was 1.46 times higher than the pure blend. The activation energy of electrical conductivity decreases as temperature increases, and the PVA/CG/7wt% nCS sample had the lowest activation energy of conduction (0.3495 eV). The semiconducting behaviour of the blend nanocomposites was explained by the skewed semi-circular arc observed in Nyquist plots. The tensile strength of 5wt% nCS loaded blend was 43.2% higher than the pure PVA/CG blend. These results suggest that this blend nanocomposite films could be a candidate for capacitors and flexible energy storage devices.

Keywords Polyvinyl alcohol · Cashew gum · Nanochitosan · Thermal properties · AC conductivity · Dielectric constant · Impedance · Tensile strength

Introduction

Polymer blends and nanocomposites constitute a novel class of functional materials with many astonishing features and thus, a wide range of applications [1–3]. Blending with different polymers can efficiently integrate the properties of distinct polymers. Improved compatibility between the constituent polymers in a blend is a crucial issue to be addressed during blending, and studies on this topic have grown in significance in recent years [4, 5]. In polymer blends, the hydrogen bonding between the component polymers is crucial for achieving a better balance of mechanical properties.

Biopolymers, particularly polysaccharides and cellulose, contain a large number of polar groups in their main chains, and their blends are frequently found to be miscible. Moreover, the growing concerns about environmental safety, waste disposal, and the extinction of resources have also turned the focus of the scientific community towards biopolymers over petroleum-derived ones [6, 7].

Novel materials obeying the green chemistry rules have begun to conquer various fields of everyday life applications. Biopolymers have recently received a lot of attention for various electronic and electrochemical uses because of their superior processability, mechanical strength, flexibility, ability to coordinate with dopants or conducting ions, ease of availability and affordability. In addition to all these advantages, biodegradability is the most important factor in addressing the growing environmental issues. The structural and physicochemical properties can be easily tailored by blending a couple of different polymers, where the

✉ M. T. Ramesan
mtramesan@uoc.ac.in

¹ Centre for Polymer Science and Technology, Department of Chemistry, University of Calicut, Calicut University P.O., Malappuram, Kerala 673 635, India

individual polymer properties are integrated via the effective interaction existing between them [8, 9]. Abdulwahid et al. [10] studied the structural, electrical and dielectric properties of a biopolymer blend electrolyte using CS and PS as hosts, doped with varying amounts of KSCN and found that samples incorporating 40 wt% of KSCN had the highest conductivity of $2.32 \times 10^{-6} \text{ S cm}^{-1}$ at room temperature. This study evaluates the effect of nanosized chitosan on the characteristics of a PVA/CG biopolymer blend.

Polyvinyl alcohol (PVA) is a well-known water-soluble polymer owing to the presence of multiple hydroxyl groups and thus being the source of hydrogen bonding. They have many applications in various fields due to their interesting properties such as water solubility, biocompatibility, biodegradability, high mechanical strength, film forming ability, high thermal and chemical stability [11, 12]. Textiles, paper, food packaging industry, etc. have utilized these advantages of PVA to a large extent [13, 14]. Cashew gum is a natural polysaccharide obtained as an exudate from the stem bark of the cashew tree (*anacardium occidentale*) which is profusely growing in tropical and subtropical regions. It is a water soluble complex heteropolysaccharide mainly composed of galactose, glucose, rhamnose, arabinose, glucuronic acids, etc. Furthermore, CG is a unique biopolymer due to its non-toxicity, biodegradability, biocompatibility, and wide availability [15, 16].

The urge to develop high-performance polymer-based materials has brought about the idea of polymer nanocomposites, where the excellence of nanotechnology is effectively utilized in the polymer world. Polymer nanocomposites typically consist of nanofiller (nanosheets, nanoplates, nanorods, nanopowder, etc.) dispersed in a polymer matrix. The most intriguing aspect of these organic–inorganic hybrid materials is the fascinating features endowed when the nanoworld meets the macroworld [17, 18]. It has been proven undoubtedly that the incorporation of very small amounts of nanoparticles into a polymer matrix can bring excellent electrical, dielectric, mechanical, thermal and optical properties. This is because of the high surface-to-volume ratio of nanofillers and their well-formed interfaces [19].

Chitosan (CS) is one of the most studied biopolymers and it is the deacetylation product of chitin, a major constituent of the shells of crustaceans such as crabs and shrimp [20]. Chemically, chitosan is a polymer with the monomer units β -1,4-D-glucosamine and N-acetyl- β -1,4-D-glucosamine. It is a linear cationic heteropolysaccharide characterized by its non-toxicity, biodegradability, and solubility in acidic media [21, 22]. Selim et al. [23] reported the dye adsorption and thermal stability of nanochitosan reinforced acrylic fiber. Cazon et al. [24] found that the addition of cellulose increases the mechanical properties of PVA/chitosan nanocomposites. Srinivasa et al. [25] studied

the properties and sorption behaviour of PVA/chitosan films. The thermal, mechanical and electrical properties of nanochitosan incorporated polymethyl methacrylate-based composites are evaluated by Shyli et al. [26]. From the literature, the PVA/CG/nCS nanocomposites have not previously been introduced, leaving room to prepare these blend nanocomposites for a plethora of uses. Thus, the present work aimed to develop PVA/CG/nCS nanocomposites with different fill levels of nCS using the solution casting procedure using water as the green solvent. The FTIR, XRD, SEM, and a universal testing machine are used to evaluate the structural, crystalline, morphological, and mechanical properties of the blend nanocomposite films. Besides, the AC conductivity, dielectric parameters, impedance and electric modulus spectra were also analysed at different temperatures.

Experimental

Materials

PVA was procured from Sigma Aldrich ($M_w = 40,000$, 87–90% hydrolysed). CG was collected from the bark of cashew trees grown in the Calicut University campus during the summer season. nCS (~50 nm) was obtained from Sigma Aldrich. Acetic acid (99.8% purity) and ethanol (95% purity) was obtained from Hi-media, India. All the chemicals used here are of analytical grade and further purification was not required. Water is used as a solvent throughout the experiments after its double distillation.

Extraction and Purification of Cashew Gum

The exudate gum collected from the bark of cashew trees was dissolved in the required amount of double distilled water. All the impurities were discarded via repeated filtration and pure cashew gum solution was then treated with 95% ethanol in a 1:3 (v/v) ratio to precipitate purified cashew gum. The precipitated CG was drained and washed twice with ethanol. It was then dried until a constant weight was attained and the purified CG was ground into a fine powder and stored in an airtight vial for further use.

Preparation of PVA/CG/ x wt% nCS Nanocomposite Films

PVA/CG (1:1)/x wt% blend nanocomposite films were prepared by an easy and economical solution casting method. For this, 5 g of PVA was dissolved in 100 mL of water at 90 °C and 5 g of CG was dissolved in 100 mL of water at room temperature. To the clear PVA solution, the CG solution was dropped slowly under magnetic stirring at room

temperature. To prepare nanocomposite films, a calculated weight percentage of (0, 3, 5, 7 and 10 wt%) chitosan nanopowder dispersed in a minimum amount of 2% acetic acid via ultrasonication was added to the PVA/CG blend solution after 4 h mixing. The resultant PVA/CG/nCS blend nanocomposite solution was stirred overnight at room temperature with subsequent ultrasonication. It was then carefully transferred to a clean petri dish, removing bubbles if any and kept for drying in a hot air oven. After 48 h, the dried films were peeled from the petri dish, weighed, and again dried until they retained a constant weight. These films were then stored in a desiccator before further analysis. Scheme 1 shows a graphic illustration of the development of a biopolymer blend nanocomposite.

Characterization

FT-IR measurements were performed with a JASCO 4100 FT-IR spectrometer in the range of 400–4000 cm^{-1} with a resolution of 4 cm^{-1} . The crystallographic arrangements of the prepared samples were analysed using X-ray diffractometer (model X'pert 3 Powder) at a scanning rate of 2°/min. FE-SEM (field emission scanning electron microscopy; Carl Zeiss, VP500 model) was used to study the morphology of fabricated blend nanocomposites, images were taken at a magnification of 20 KX. Differential scanning calorimeter (model Netzsch DSC 204 F1 Heat flux DSC) analyses were performed to study the different thermal transitions associated with samples at a heating rate of 10 °C per min in a temperature range of 30 to 300 °C in an inert atmosphere (N_2). The thermal decomposition profile of polymer composites was carried out in a Hitachi STA7200 thermogravimetric analyser at a heating rate of 10 °C per min. The electrical conductivity and dielectric properties of blend nanocomposite films (circular in shape, 0.3–0.5 mm thickness, 1.2 cm diameter) were tested using a Hioki impedance analyser (HIOKI 3570 model) at an applied potential of 1 V in the frequency range of 100 to 10^6 Hz at different temperatures

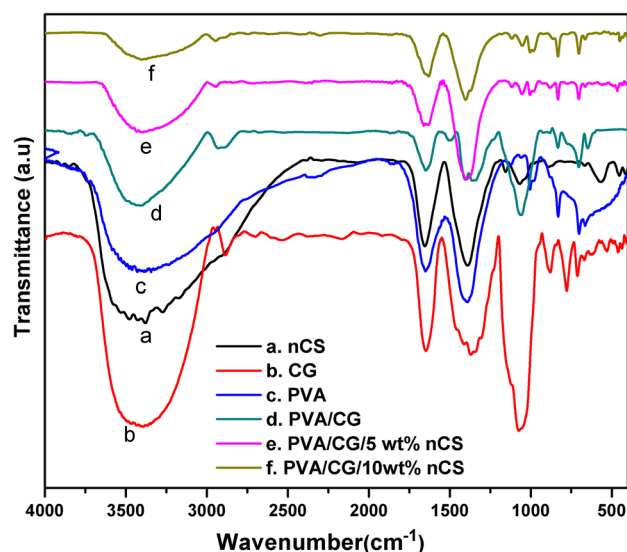


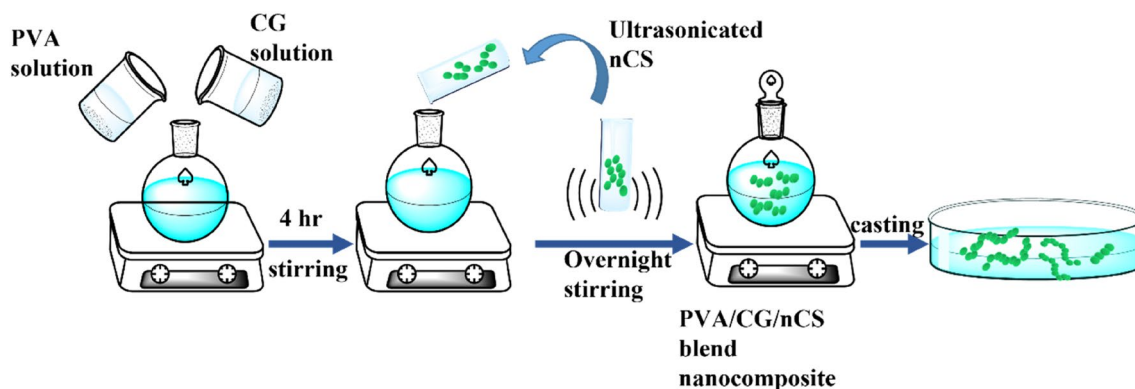
Fig. 1 FTIR spectra of PVA, CG, PVA/CG, nanochitosan and its nanocomposites

(30–90 °C). The tensile strength and elongation at break of the biopolymer blend nanocomposite films were determined using an Instron instrument according to ASTM D-882. Film strips were stretched at a cross-head speed of 10 mm per min. A Shore A-type durometer was used to gauge the hardness of the samples as per ASTM D-2240.

Results and Discussions

FTIR

FTIR is an efficient tool to confirm the interactions present between the constituents of blend nanocomposites and the structural changes that have occurred to the PVA/CG blend after nCS inclusion. Figure 1 represents the FTIR spectra of nCS, PVA, CG, PVA/CG and nanocomposites.



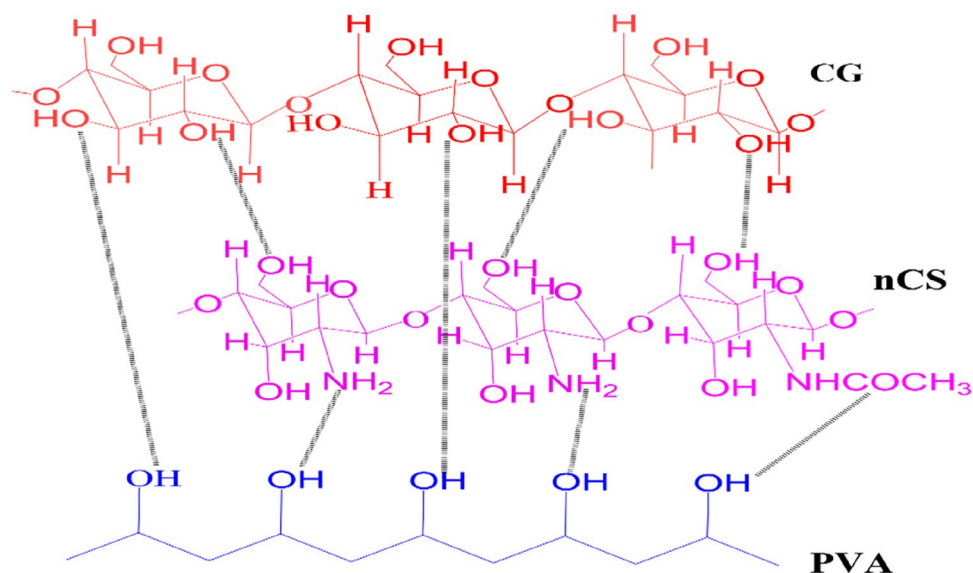
Scheme 1 Preparation of PVA/CG/nCS blend nanocomposites

Table 1 Characteristic IR bands of PVA, CG, nCS, PVA/CG and its nanocomposites

Samples	Peak position (cm ⁻¹)	Assignment of peak	References
PVA	3390	OH stretching	[27]
	1640	Deformation of OH of water	
CG	3409	OH stretching	[27]
	2886	CH stretching	
	1653	C=O stretching from glucuronic acid	
	1416	CH ₂ scissoring	
	1072	C–O–C stretching of pyranose ring	
PVA/CG	3424	OH stretching	[27, 28]
	2934	CH stretching	
	1649	C=O stretching from glucuronic acid	
nCS	1059	C–O–C stretching of pyranose ring	[29]
	3427	OH and NH stretching	
	1637	Amide II stretching	
PVA/CG/5 wt% nCS	1389	Amide III stretching	
	3401	OH and NH stretching	
	2945	CH stretching	
	1647	C=O stretching from glucuronic acid	
PVA/CG/10 wt% nCS	1397	Amide III stretching	
	3390	OH and NH stretching	
	2940	CH stretching	
	1640	C=O stretching from glucuronic acid	
	1394	Amide III stretching	

The characteristic vibration bands of each of them are tabulated in Table 1. The OH stretching band of pure PVA and pure CG is indexed at 3390 cm⁻¹ and 3409 cm⁻¹ are shifted slightly to a higher wavenumber of 3424 cm⁻¹ for pure PVA/CG blend. This can be attributed to the hydrogen bonding between the polar groups of PVA and CG [27]. Additionally, the IR spectrum of PVA/CG allocates CH stretching from sp³ carbon at 2934 cm⁻¹ and the carbonyl group from the glucuronic acids of CG at 1649 cm⁻¹. The C–O–C stretching vibration of the glycosidic bond of the pyranose

ring is found at 1059 cm⁻¹ [15, 28]. After the inclusion of nCS in the PVA/CG blend, these characteristic peaks are observed to shift slightly, indicating the interfacial interactions between the nCS and PVA/CG blend. For 5 wt% and 10 wt% nanocomposites, the OH stretching vibration is shifted to a lower frequency range of 3401 cm⁻¹ and 3390 cm⁻¹ respectively. Other characteristic peaks of nCS are also found in the FTIR of nanocomposites and some peaks that are common to both blend and nCS appear with a slight shift in their peak position and small changes in broadness [29].

Scheme 2 Plausible interactions present in PVA/CG/nCS blend nanocomposite

All these observations confirm the possibility of effective interactions between the components of the system. Plausible interactions present in the blend nanocomposite is shown in Scheme 2.

XRD

The XRD patterns of pure CG, pure PVA, nCS, PVA/CG blend and its nanocomposites is given in Fig. 2. Pure PVA film shows a semicrystalline reflection at $2\theta = 19.7^\circ$ with a shoulder at 22.9° and a small peak at 41.09° [30]. The amorphous nature of purified cashew gum powder is evident from the major diffraction peak at $2\theta = 19.3^\circ$ [31].

Blending of PVA and CG retains the broad diffraction peak at 19.49° and the hump at 40.62° . The XRD of nCS shows diffraction peaks at 19.93° , 29.43° and less intense peaks in the range of 35° to 49° [32]. Interestingly, diffraction patterns of blend nanocomposites show the major crystalline peaks of nCS along with the peak of PVA/CG with reduced broadness. Moreover, this peak is slightly shifted to a higher theta value in the nanocomposite. For example, the broad diffraction peak of PVA/CG at $2\theta = 19.49^\circ$ is shifted to 19.63° and 19.73° for 5 and 10 wt% samples, respectively [33]. The intensity of the peak corresponding to nCS in the nanocomposite increases with its concentration. Crystallinity index, FWHM, d-spacing of major peaks of the individual polymers, nCS, PVA/CG blend and 5, 10 wt% nCS

Table 2 FWHM, d-space and crystallinity index of PVA, CG, nCS, PVA/CG blend and its nanocomposites

Samples	2θ (degree)	FWHM	d- space (Å)	Crystallinity index (%)
PVA	19.79	2.12	1.69	15.38
	41.09	2.32	0.39	
CG	19.30	4.99	3.45	12.76
	40.62	1.62	0.77	
PVA/CG	19.49	3.42	2.45	14.97
	40.62	1.62	0.77	
nCS	19.93	2.87	1.49	22.74
	29.43	0.51	0.92	
PVA/CG/5 wt% nCS	19.63	3.09	2.02	18.08
	29.81	0.88	1.07	
	40.60	1.75	0.77	
PVA/CG/10wt% nCS	19.73	2.37	1.81	19.44
	29.76	0.65	1.04	
	40.94	2.37	0.77	

loaded samples are given in Table 2 [34]. It is clear from the table that the addition of nanofiller to the blend caused some variation in d-space and crystallinity. All these observations suggest the uniform arrangement of the nanofiller as well as the interactions between the polymer chains of PVA/CG and nCS. These observations are consistent with the result from FTIR.

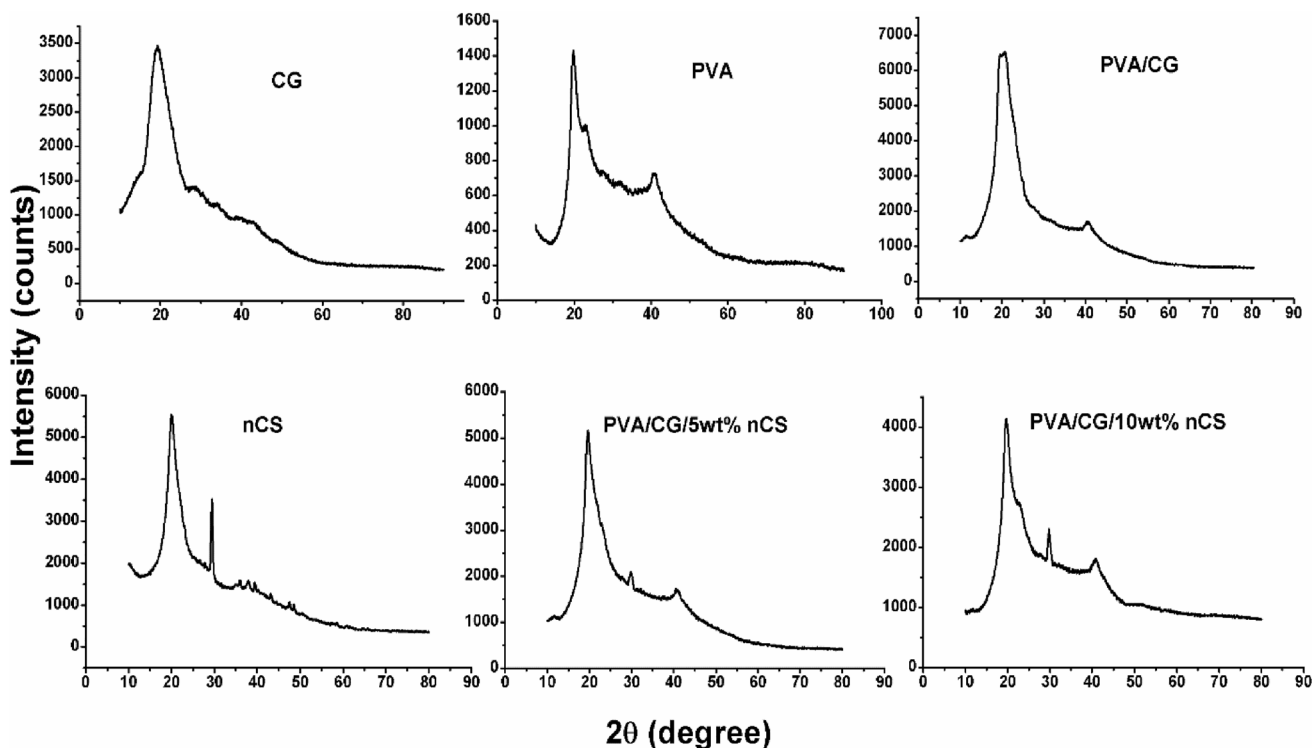


Fig. 2 XRD pattern of CG, PVA, PVA/CG, nCS, PVA/CG/5 and 10wt% nCS

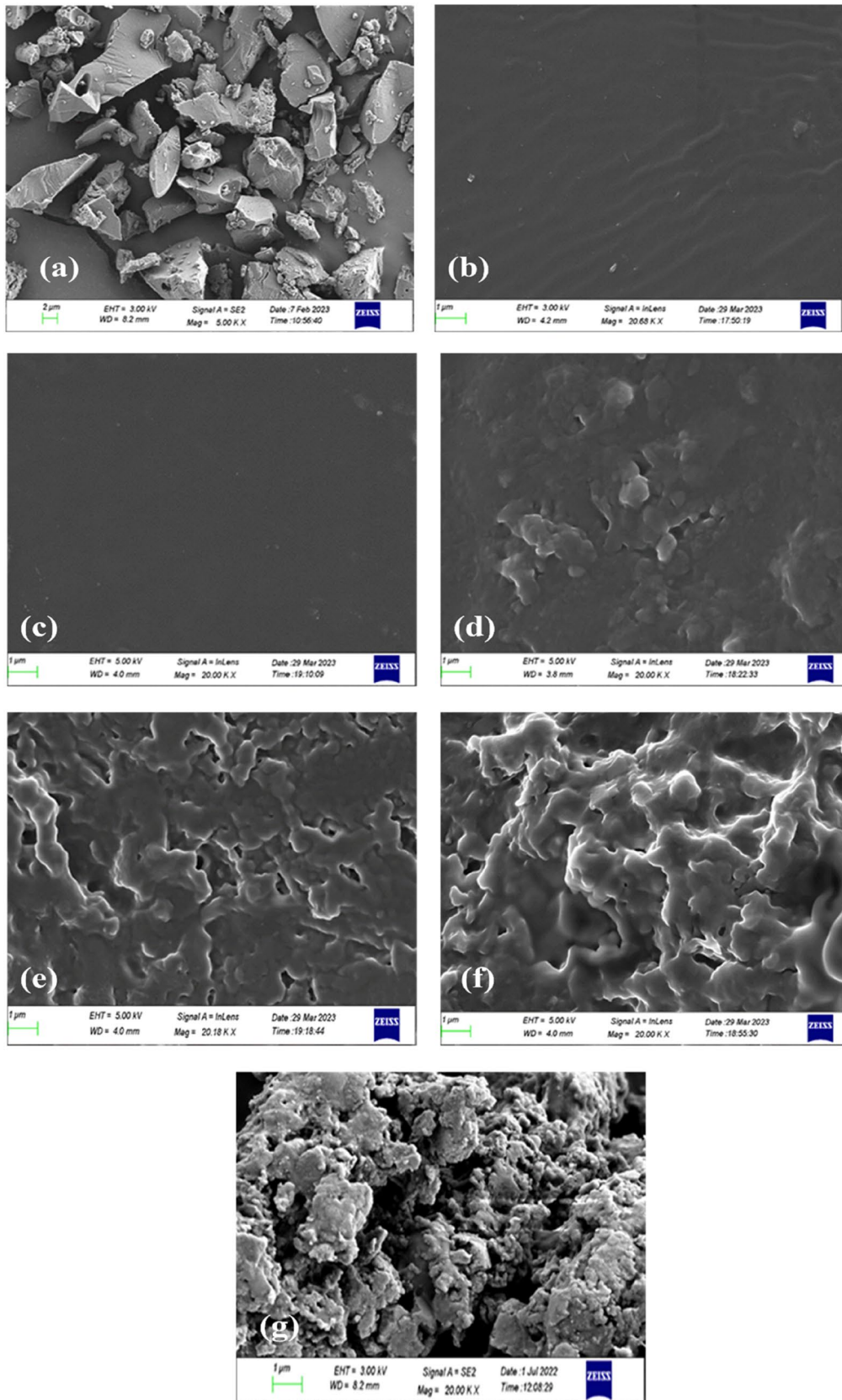


Fig. 3 SEM images of **a** CG **b** PVA **c** PVA/CG **d** PVA/CG/3 wt% nCS **e** PVA/CG/5wt% nCS **f** PVA/CG/7wt% nCS and **g** PVA/CG/10 wt% nCS

SEM

Surface features of CG, PVA, pristine PVA/CG blend and its nanocomposites are monitored by SEM analysis and the micrographs are displayed in Fig. 3. Figure 3a shows the SEM image of purified CG powder with various particle sizes having rough surfaces. Virgin PVA film has a nearly uniform and smooth surface, as observed in Fig. 3b. A clean, smooth and homogeneous surface morphology of pristine PVA/CG blend without any cracks and pores indicates high compatibility between these two polymers. The polar-polar interactions between PVA and CG are responsible for the compatibility of this blend. Figure 3d–g shows that the smooth surface morphology of PVA/CG is progressively disturbed as the nCS content increases. Small flakes are found in the 3 and 5 wt% nCS loaded blend, but structural integrity and uniformity are preserved to some degree. The uniform morphology observed at 7% loading suggests that the strong interaction between the fillers and the polymer blend results in a more compact structure. However, at higher loading (10 wt%) structural integrity is completely disrupted and the surface becomes rougher due to the aggregation of nanoparticles [35, 36].

Thermal Properties

TGA

The influence of nCS on the thermal stabilities of PVA/CG can be checked with TGA. The TGA thermograms of the PVA/CG given in Fig. 4A exhibit two-step degradation, while the PVA/CG/nCS films have three degradation steps. The DTG curves (Fig. 4B) show the maximum temperature

for the decomposition of films. The decomposition step below 100 °C associated with a small weight loss is present in the thermogram of all the films indicating the removal of moisture absorbed on the surface of sample and other volatile impurities [37]. For a pristine blend, the major degradation occurs in the range of 184–400 °C with a maximum weight loss rate (T_{max}) at 283 °C. Almost 55% of the weight loss here is attributed to the polymer chain scission. On the other hand, the nanocomposites exhibited a second thermal degradation within the range of 160–260 °C. It is interesting to note that the decomposition temperature increases with the addition of nCS. About 19% of the mass loss that occurred in this range can be attributed to the loss of bound water and acetic acid residue [38]. The T_{max} obtained for 3, 5, 7 and 10 wt% nCS loaded PVA/CG is observed at 212, 216, 225, and 236 °C respectively. The last and major disintegration is associated with almost 36% weight loss, starting around 283, 287, 293 and 303 °C with T_{max} at 321, 326, 333 and 338 °C for 3, 5, 7 and 10 wt% nCS loaded PVA/CG respectively. This weight loss constitutes the degradation of polymer chains of PVA and CG polysaccharides, decarboxylation and evolution of CO_2 . The addition of nCS to PVA/CG significantly increases the decomposition temperature, showing better thermal stability due to the strong interactions between them [39]. The residual weight percentage of the pristine blend after final thermal disintegration is 6.5%. The inclusion of nCS increases the residual weight percentage from 6.5% to 9.3, 10.8, 12.05 and 12.9% for 3, 5, 7 and 10 wt% nCS in the PVA/CG. These results also indicate the enhanced thermal stability of biopolymer blend nanocomposites compared to pure PVA/CG.

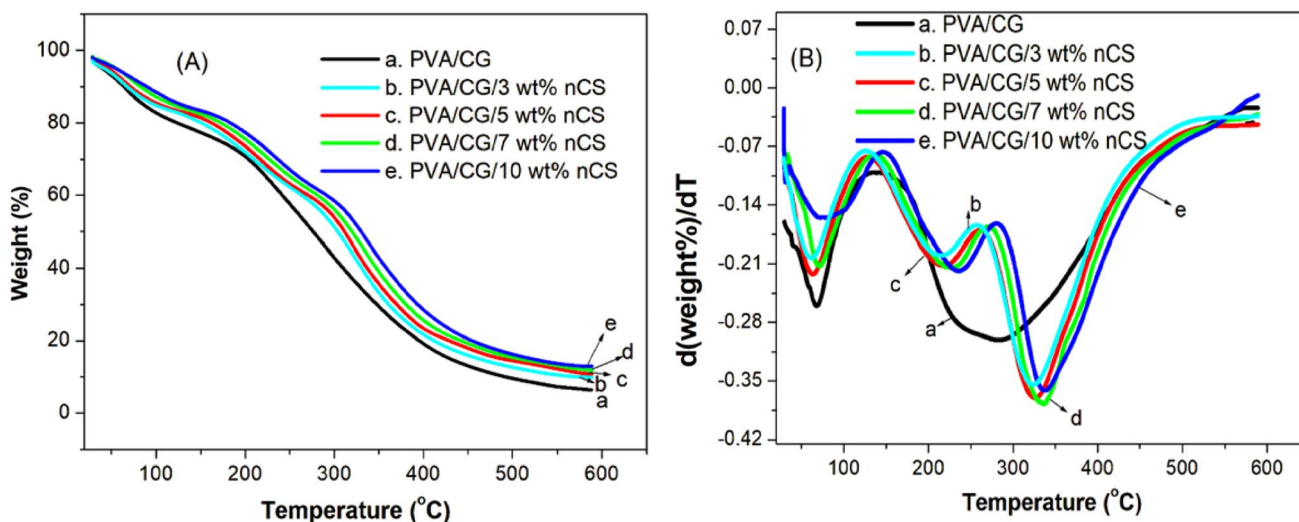


Fig. 4 A TGA and B DTG profiles of PVA/CG and nanocomposites

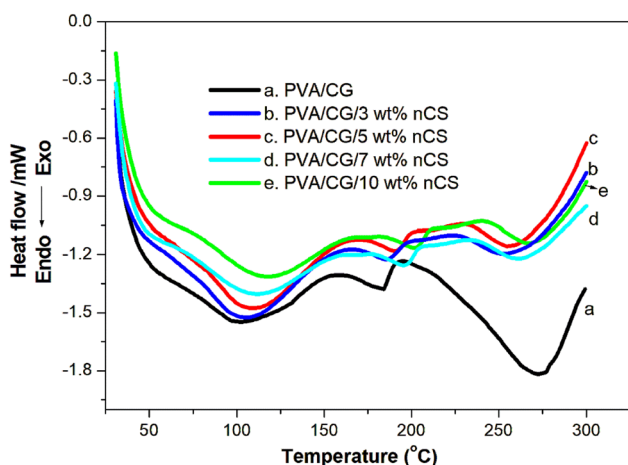


Fig. 5 DSC curves of PVA/CG and its nanocomposites

DSC

The DSC profiles of pure PVA/CG and with different nCS loadings are analysed to understand the various thermal transitions associated with them. Figure 5 shows multiple endotherms, with the one at a lower temperature corresponding to the glass transition point (T_g). A single T_g is observed for the blend, which is attributable to the miscibility of constituent polymers in the blend. However, the T_g value of PVA/CG increased from 99 to 104 °C, 108 °C, 113 °C and 118 °C for 3, 5, 7 and 10 wt% nCS inclusion, respectively. The change in T_g confirms the effective interfacial interaction through the polar groups of PVA/CG and chitosan. The increase in T_g with the addition of nCS indicates the rigidity of the prepared biopolymer blend nanocomposites [40]. The broad endothermic dip at 273 °C is the melting temperature (T_m) of the pure PVA/CG blend. The T_m of the blend is increased to 278 and 283 °C for 5 and 10 wt% chitosan loaded films, respectively. The shift in T_g and T_m values further confirms the effective incorporation of nanochitosan into the PVA/CG segments.

Electrical Measurements

AC Conductivity

The frequency dependent response of AC conductivity at room temperature and over a temperature range in polymer systems has been studied by many [41, 42]. AC conductivity can be measured by using the following relationship [42]:

$$\sigma_{ac} = \varepsilon_0 \times \varepsilon_r \times 2\pi f \times \tan \delta \quad (1)$$

where ε_0 , ε_r , $\tan \delta$ and f are permittivity of free space (8.85×10^{-14} F/cm), permittivity of sample, loss tangent or

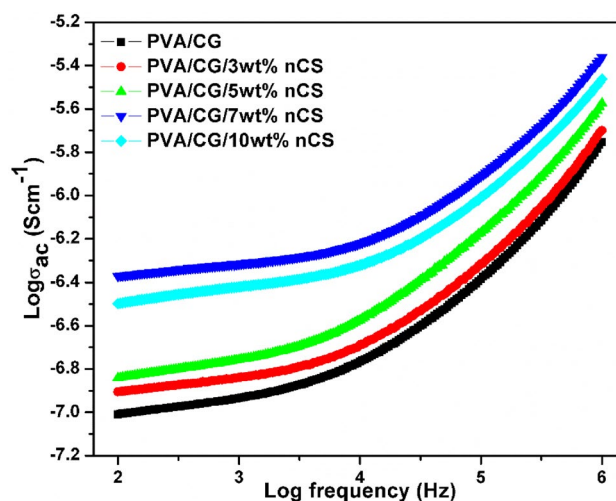


Fig. 6 Variation of AC conductivity with respect to frequency of PVA/CG and nanocomposites

dissipation factor and applied frequency, respectively [42]. Figure 6 demonstrates how the AC conductivity of the prepared blend varies with applied frequency and nano-powder loading. It is obvious from the figure that there is a gradual increase in conductivity with the addition of nCS to the PVA/CG blend. As the incorporated nanoparticles can effectively penetrate through the blend segments due to its small size, they reduce the cohesive interactions present in the polymer chain and make the matrix more flexible, resulting in enhanced segmental motion. Ion mobility through such a network is more feasible and this will lead to increased conductivity with filler loading. The H^+ ions are the major charge carriers in the system, and their number and mobility will rise after the addition of nCS to the pure blend [43]. It is important to note that dispersion, size and filler type play a major role in determining the conductivity rise. Though there is a progressive rise in conductivity up to 7 wt% nCS loading, a significant drop is observed beyond this owing to the nanoparticle agglomeration and uneven distribution in the polymer blend as evident from SEM [44]. It is interesting to note that there are two unique regions in the graph of all the studied films. A frequency-independent low-frequency zone associated with the space charge polarization arises due to the long-time residence of charge carriers at the electrode-electrode interface and a high-frequency dispersion beyond 10^4 Hz, characterized by its sharp increase in conductivity with frequency and obeying power law [33]. This increase in conductivity can be explained by hopping and Koop's model. As the frequency rises, the charge carrier hops quickly from one transit site to another within the polymer network. According to Koop's,

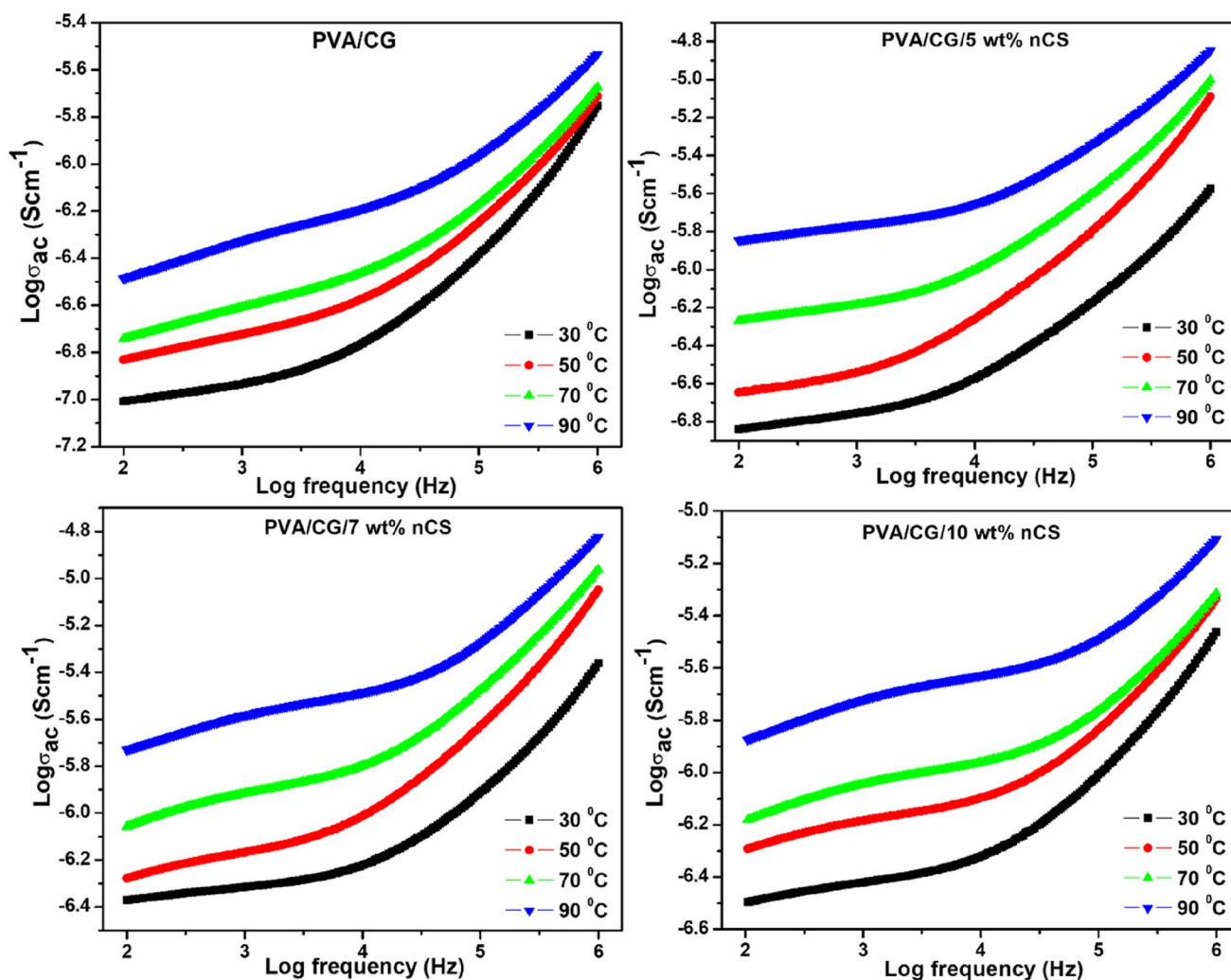


Fig. 7 Temperature-dependent variation of AC conductivity of blend and its nanocomposites

relatively resistive grain boundaries form at low frequencies, causing small conductivity values [45].

The temperature-dependent variation of AC conductivity is portrayed in Fig. 7. Here we analyse the conductivity changes over a temperature range of 30 to 90 °C as a function of frequency for the pristine blend and its nanocomposites. As expected, a positive variation of conductivity with temperature is obtained. It is a well-known fact that thermal energy causes the charge carriers to acquire high mobility and cross the energy barrier for electrical conduction. This eventually results in enhanced conductivity at higher temperatures, an important feature to be utilized in various device applications [44].

High frequency dispersion above 10⁴ Hz is observed at all temperatures and where the system holds a universal power law [46],

Table 3 Frequency exponent ‘s’ at various temperature for PVA/CG and its nanocomposites

Loading of nCS (wt%)	Frequency component ‘s’			
	30 °C	50 °C	70 °C	90 °C
0	0.4975	0.4284	0.3947	0.3284
3	0.4869	0.4332	0.3762	0.3653
5	0.4893	0.4695	0.4593	0.4042
7	0.4775	0.4250	0.4241	0.3383
10	0.4286	0.3834	0.3249	0.2561

$$\sigma_{ac}(\omega T) = A(T)\omega^s \tag{2}$$

where σ_{ac} , ω and A are the frequency and temperature dependent AC conductivity, angular frequency ($2\pi f$) and temperature-dependent constant respectively. ‘s’ is an exponent, a dimensionless quantity that depends on both

frequency and temperature having values in the range $0 \leq s \leq 1$ [46]. Values of ‘s’ obtained from the slope of the plot $\log \sigma_{ac}$ vs $\log \omega$ are listed in Table 3. For all the films ‘s’ is fall in the range 0.25–0.5, non- zero values ‘s’ is an indication of the non-Debye nature of prepared biopolymer blend and nanocomposites. Moreover, the value of exponent s is found to drop with temperature rise, which implies the Correlated Barrier Hopping (CBH) model of electrical conduction persists in the system. According to the CBH model, electrical conduction in the system arises due to the hopping of charge carriers from one transit site to another over the potential barrier separating them [47].

Arrhenius Plots

Conductivity enhancement with temperature rise can be explicitly proved by the Arrhenius plots, where $\log \sigma_{ac}$ is drawn against $1000/T$. Figure 8 displays the Arrhenius plot

Table 4 E_a of PVA/CG and its nanocomposites at various frequencies

Samples	Activation energy for electrical conduction (eV)		
	10^2	Frequency (Hz) 10^4	10^6
PVA/CG	1.6466	1.4807	1.1110
PVA/CG/3wt% nCS	1.0528	1.0110	0.8334
PVA/CG/5wt% nCS	0.8156	0.7592	0.6592
PVA/CG/7wt% nCS	0.7787	0.6095	0.3495
PVA/CG/10wt% nCS	0.8971	0.8009	0.5396

for PVA/CG and its nanocomposites. The negative slope obtained here indicates that conductivity increases with increasing temperature. In addition, the slope is equivalent to activation energy (E_a) for electrical conduction and the

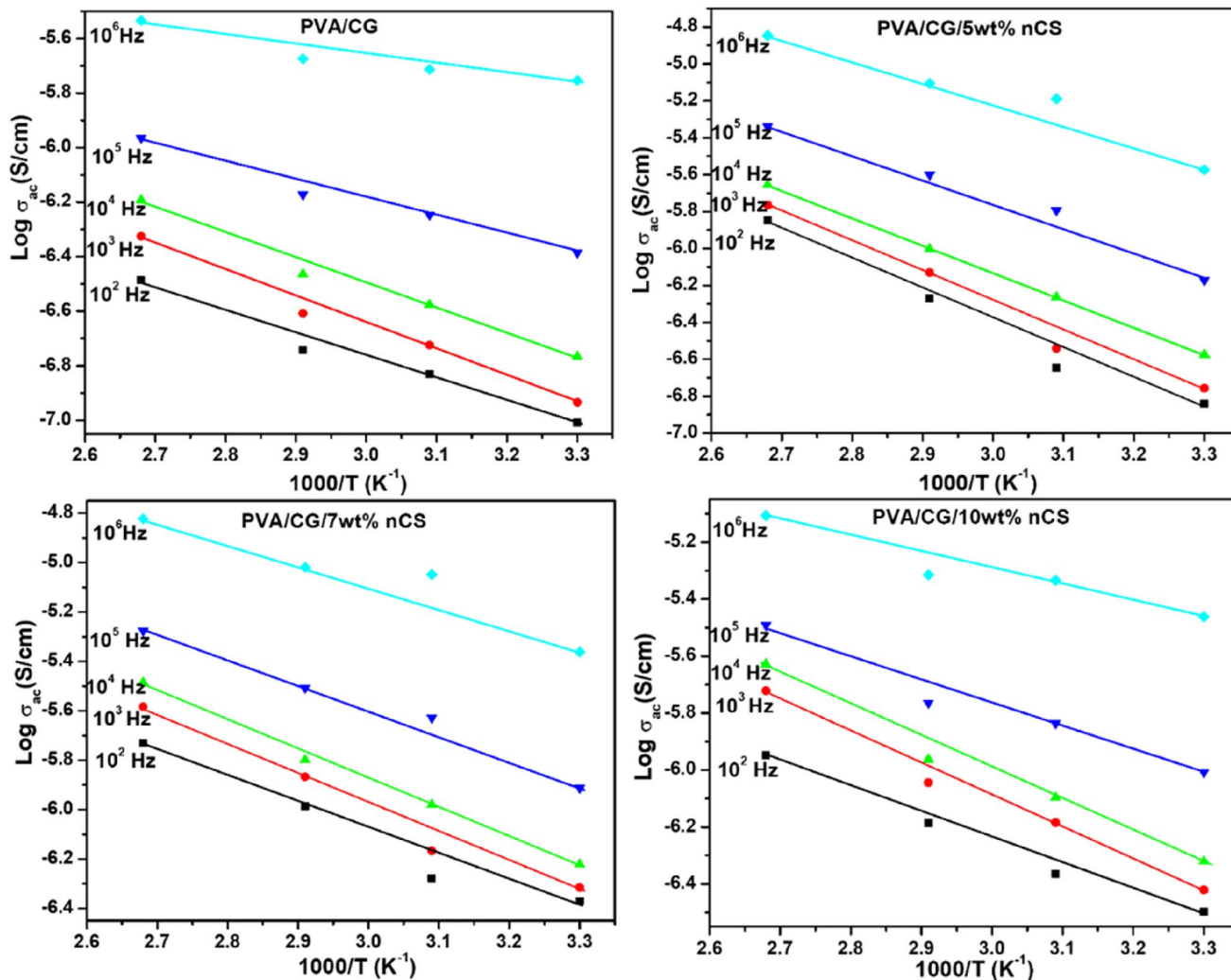


Fig. 8 Arrhenius plots of PVA/CG and nCS loaded PVA/CG

values at a particular frequency for all the samples are given in Table 4.

At all frequencies, the minimum E_a for electrical conduction is obtained for 7 wt% nCS incorporated PVA/CG, indicating its highest conductivity and it agrees with the forementioned results [48].

Dielectric Constant

The dielectric constant (ϵ') describes the amount of charge that a material can hold. Evaluation of the dielectric constant is necessary to understand its use in storage applications. It can be calculated by the following relationship [49].

$$\epsilon' = C_p d / A \epsilon_0 \tag{3}$$

where C_p , d , A and ϵ_0 are capacitance, the thickness of the film, the area of the cross-section of the film sample and permittivity of free space (8.85×10^{-14} F/cm) respectively [49].

The dielectric response of the prepared blend and its nanocomposites is studied as a function of frequency at room temperature and the results are depicted in Fig. 9. The ϵ' of all the films are high at low frequency whereas towards the high frequency region it rapidly drop and gradually achieve a frequency independent nature, as observed from the figure. The large value of dielectric constant is attributed to the dipolar and interfacial polarization at low frequency. This is due to the sufficient time available for the dipoles to orient in the applied field. On the other hand, the rapidly changing field at higher frequency does not provide enough time for dipole alignment and hence ϵ' decreases [50]. It is clear from the figure that the dielectric constant has a positive relation

with nCS loading. This increase in ϵ' with an increase in nCS concentration up to 7 wt% and the decrease beyond that loading is noteworthy. Many dipoles are present in the biopolymer system, like the PVA/CG blend. After nCS loading, the number of dipoles will again increase and the interaction between nCS and PVA/CG blend chain leads to the dipolar ordering of polar groups in it, which eventually leads to an increased dielectric constant. The optimum ϵ' value is shown by PVA/CG/7wt% nCS film. The low value obtained at 10 wt% nCS loading is owing to the agglomeration of nanoparticles in the PVA/CG blend matrix [49].

Figure 10 demonstrates the variation of dielectric constant with temperature. In this temperature range (30–90 °C) of study, the dielectric constant is significantly increased as the temperature increases from 30 to 90 °C. With the rise in temperature, the dissociation and pre-dissociation of coupled charges in the system will result in an increment in the free charge carriers. Thus, at low frequencies, the charge remains at the interface, increasing the dielectric constant [51]

Electric Modulus Study

Electric modulus analysis is an effective tool to investigate the relaxation process in polymer composites and polymer nanocomposites. Modulus is a complex function expressed as given below [52].

$$M = M' + jM'' \tag{4}$$

The real part M' is obtained from $M' = \frac{\epsilon'}{(\epsilon')^2 + (\epsilon'')^2}$ and the imaginary part is obtained from following equation

$$M'' = \frac{\epsilon''}{(\epsilon')^2 + (\epsilon'')^2}$$

The change in real (M') and imaginary (M'') modulus with respect to the frequency at various temperatures for PVA/CG and 7wt% nCS loaded PVA/CG is drawn in Fig. 11.

At low frequencies, the real modulus M' of the pristine blend and its nanocomposite is zero at all temperatures. This long tail end parallel to the X axis is transformed into a noticeable hike towards higher frequency. This confirms the high capacitance and significant electrode polarization at low frequencies and the elimination of electrode polarization at higher frequencies. As the temperature increases, the real modulus M' is found to decrease gradually [52, 53]. Imaginary modulus (M'') spectra show both the pristine blend and nanocomposite tend to merge at zero M'' at low frequencies and at temperatures. While a relaxation peak is observed towards high frequency and these well-defined peaks shift to the right with an increase in temperature, indicating a decline in relaxation time for conduction as per the equation $\tau_m = 1/2\pi f_m$. This result is consistent with

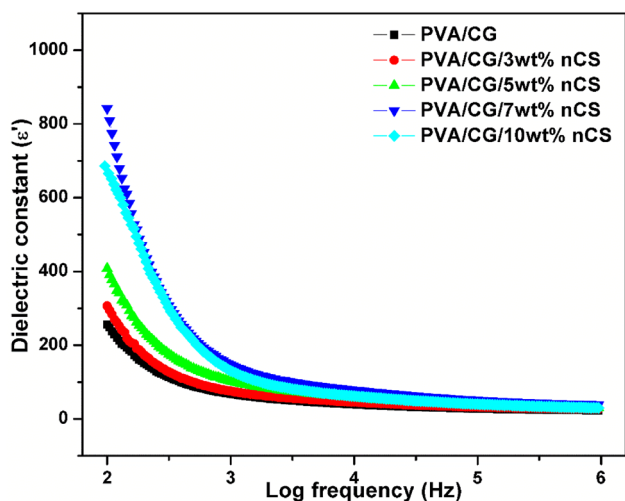


Fig. 9 Variation of dielectric constant of PVA/ CG/ nCS nanocomposites

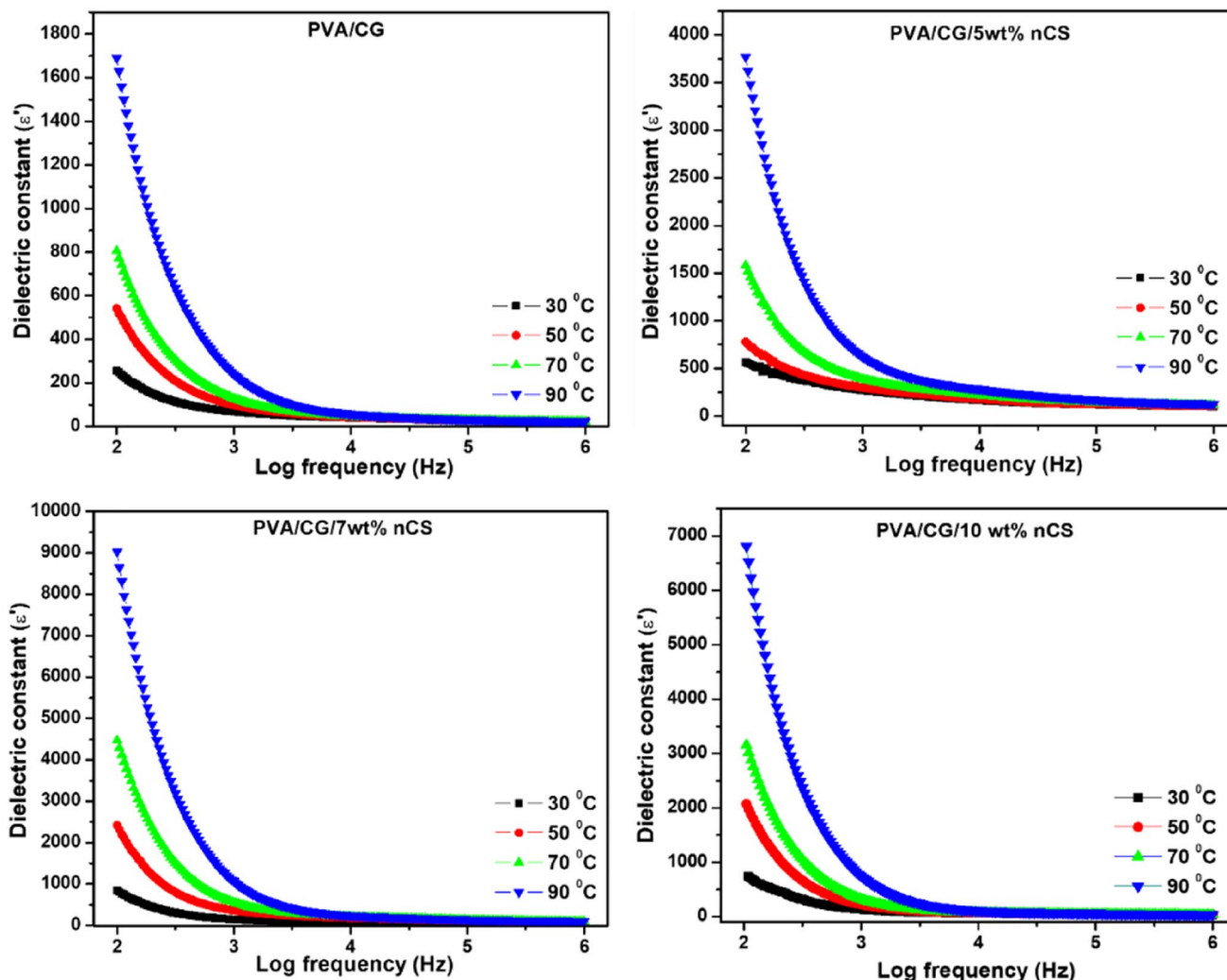


Fig. 10 Variation of dielectric constant with frequency and temperature

those obtained from temperature dependent conductivity studies, as the temperature rise will improve the segmental mobility of the polymeric chain, the transport of charge carriers through which is easy and hence the conductivity will be enhanced with the temperature [45].

Impedance Analysis

Impedance is the resistance that a conducting material offers to alternating current and impedance analysis has been an important method to evaluate the electrical properties of polymer nanocomposite. Impedance is a complex function Z^* , it can be evaluated from the relation [54],

$$Z^*(\omega) = (Z' - iZ'') \quad (5)$$

where, $Z' = |Z|\cos\theta$ and $Z'' = |Z|\sin\theta$

The dependence of the real (Z') and imaginary (Z'') part of impedance with frequency at temperatures ranging from 30 to 90 °C for PVA/CG and PVA/CG/7wt% nCS is depicted in Fig. 12. The real impedance is higher at low temperatures and low frequencies. There is a significant decrease in Z' with an increase in temperature and at higher frequency Z' tends to zero irrespective of temperature. The relaxation process prevalent in the prepared biopolymer blend is evident from the single maximum appearing in the log frequency vs Z'' plot. As the temperature increases, the height of maxima decreases and subsequently shifted to a higher frequency, indicating a reduction in relaxation time [54].

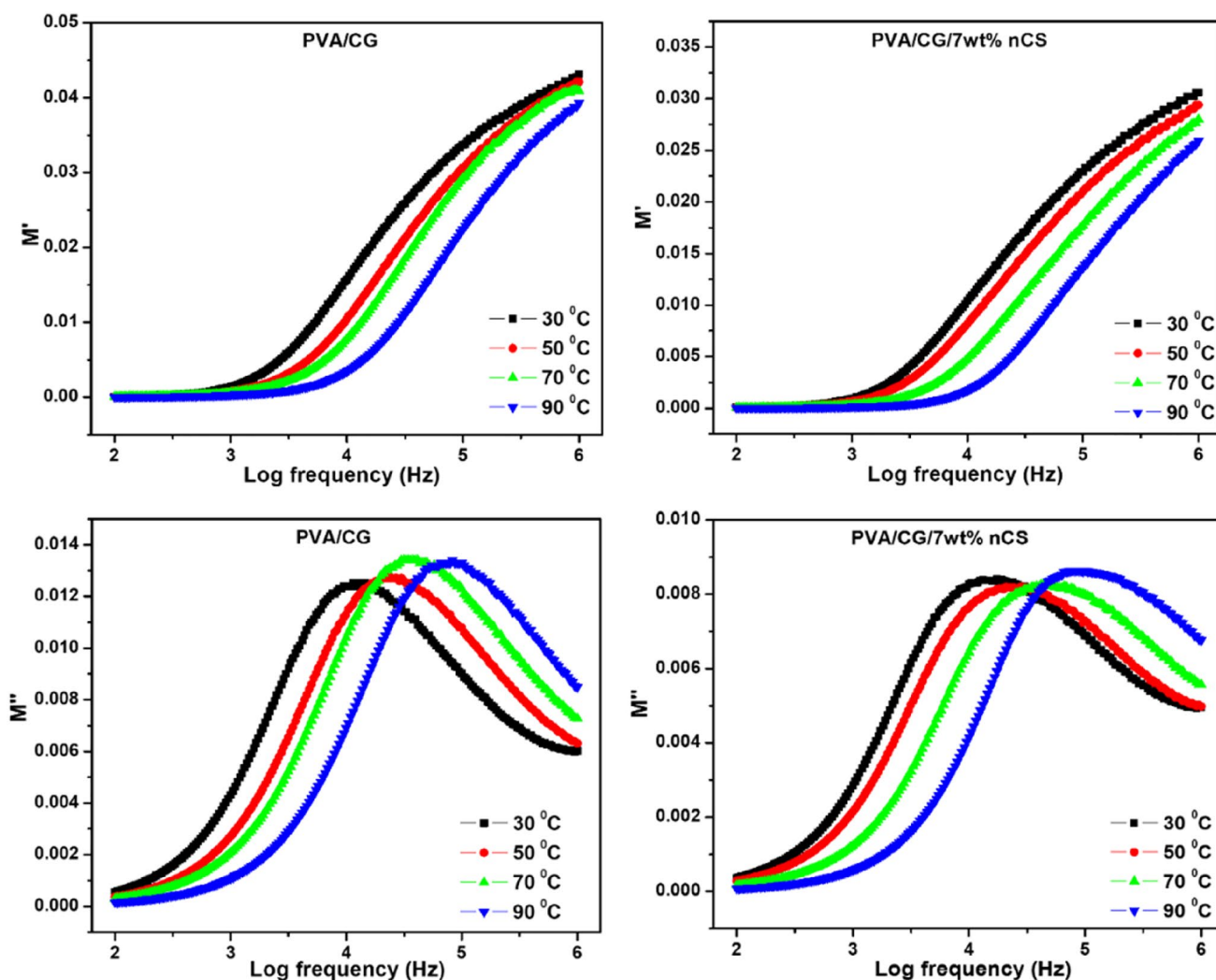


Fig. 11 Electric modulus spectra of PVA/CG and PVA/CG/7 wt% nCS

Nyquist Plot

The Z' vs Z'' plot of PVA/CG and nCS loaded PVA/CG at various temperatures is shown in Fig. 13. The Nyquist plots of all the films look similar, with a high frequency semicircle and a small spike at low frequency. The semi-circular region corresponds to the parallel combination of bulk resistance (R_b) and bulk capacitance. R_b is obtained from the intercept of a semicircle at the X-axis. DC conductivity (σ_{dc}) of the films can be determined using the relation given below [55].

$$\sigma_{dc} = \frac{1}{R_b} \times \frac{t}{A} \tag{6}$$

where A and t are the surface area and thickness of the film. The computed R_b and σ_{dc} values for all the prepared films at room temperature are listed in Table 5, lowest R_b and highest σ_{dc} is found for 7 wt% nCS loaded blend nanocomposite. As

per Nyquist plot, the equivalent circuit model to represent the electrical properties of prepared blend nanocomposite is drawn in Fig. 14. This circuit is composed of a parallel combination of resistor R_b and capacitor C_1 in series with capacitor C_2 [47, 55]. It is obvious from the figure that the radius of the semicircle decreased with an increase in temperature. This implies a negative temperature coefficient of resistance, i.e., the conductivity has a direct correlation with temperature [56]. The small spike found in the low-frequency range is attributed to the double-layer capacitor formed at the electrode-sample interface where the charge carriers accumulate and cannot tunnel through the interface. So, the charge carriers possess high impedance and low mobility, which results in decreased electrical conduction at low frequencies [47].

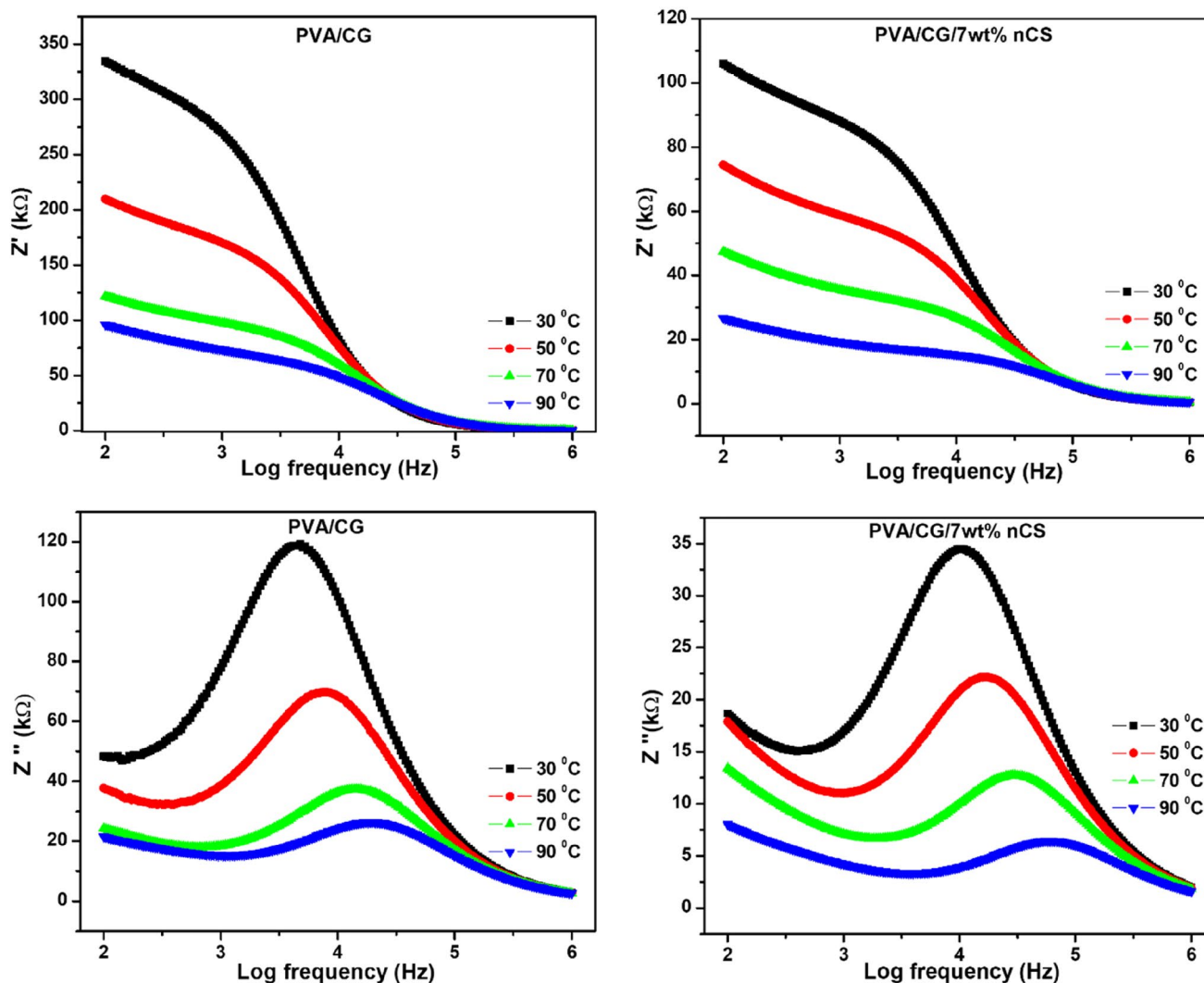


Fig. 12 Variation of Z' and Z'' with frequency at different temperature

Mechanical Properties

Investigation of the mechanical attributes of films is exclusively important, as knowledge of the maximum stress that the film can withstand without breakage and elongation at fracture are crucial aspects in many applications. Tensile strength, elongation at break (EB) and hardness of the prepared PVA/CG blend and various contents of nCS incorporated PVA/CG blend nanocomposites are summarized in a bar diagram shown in Fig. 15. Figure 16 presents the stress–strain curve of the prepared films. The tensile strength of pristine PVA/CG is 31.44 MPa, which increases with the addition of nCS. The PVA/CG bend 5 wt% sample exhibited the highest tensile value (45.02 MPa) among all the prepared films. This indicates not only the reinforcing effect of nCS but also the effective dispersion and effective interfacial adhesion between nCS and PVA/CG blend

chain. The possibility of strong hydrogen bonding and electrostatic interactions between the components of this ternary system is already confirmed by FTIR and XRD [57, 58]. It is interesting to note that there is a 43.2% increase in the TS while incorporating 5wt% nCS. A small drop in TS at higher loadings can be due to the high agglomeration rate of nanoparticles. The parameter EB suggests the stretching capability of films, it is found to be 195% for pure blend whereas nCS addition slightly reduces film elongation. This suggests the fragility of films upon nCS addition as it can act as a stress concentrator and promote premature wreckage. By adding 10 wt% nCS, the EB is decreased to 169%, which further confirms the reinforcing effect of nCS [59]. The effect of nCS on the mechanical performance of the prepared films is also evident, as it induces an appreciable increase in the hardness of the nanocomposite films [36, 60].

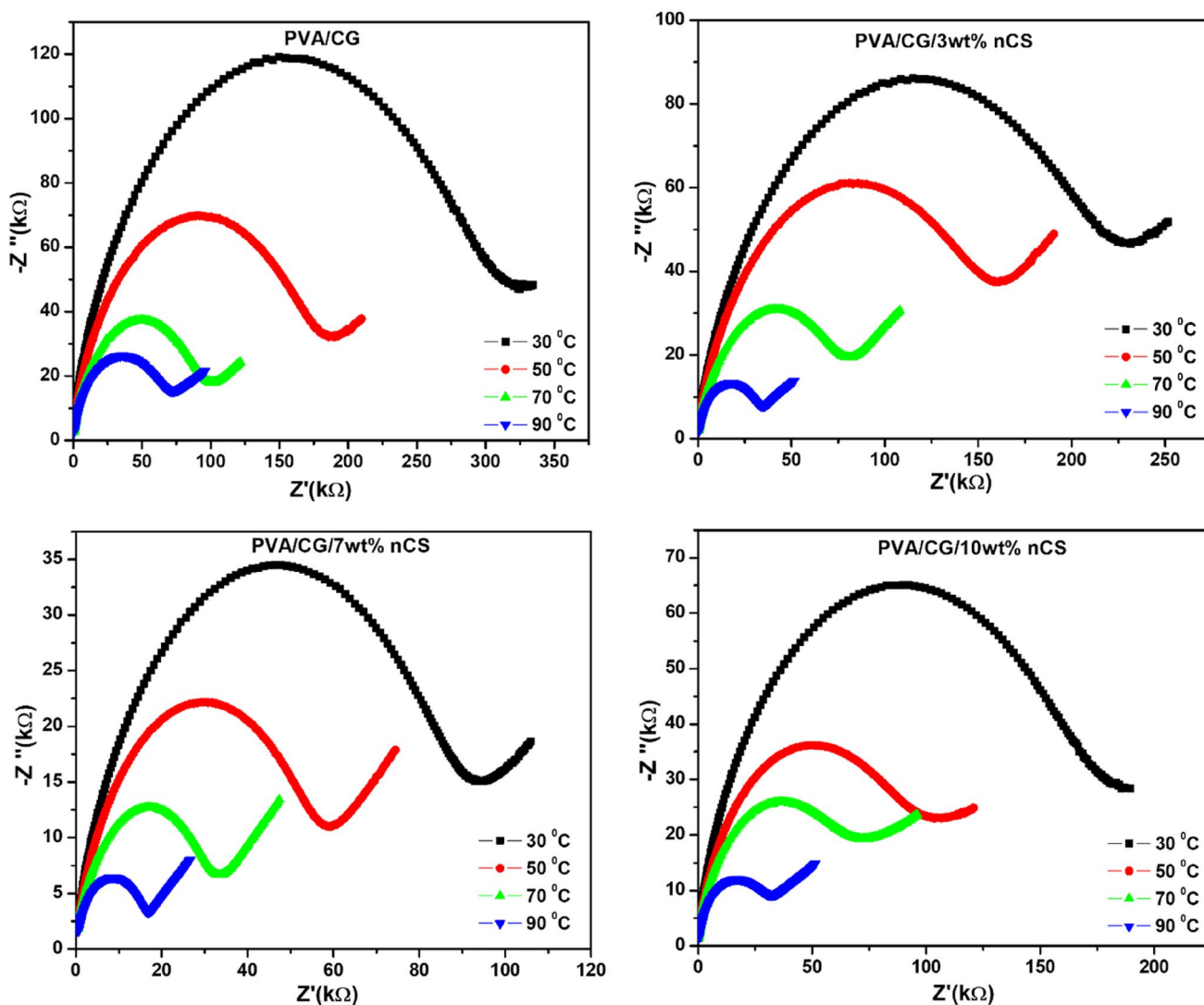


Fig. 13 Nyquist plot of PVA/CG and its nanocomposites at various temperatures

Table 5 R_b and σ_{dc} determined from Nyquist plot at room temperature

Samples	R_b (kΩ)	σ_{dc} (Scm ⁻¹)
PVA/CG	322	9.68944×10^{-8}
PVA/CG/3wt% nCS	224	1.41638×10^{-7}
PVA/CG/5wt% nCS	190.6	1.89822×10^{-7}
PVA/CG/7wt% nCS	92.37	3.87269×10^{-7}
PVA/CG/10wt% nCS	178.5	2.09546×10^{-7}

Conclusion

In summary, we have developed a completely bio-friendly blend nanocomposite films based on PVA and CG with various concentrations of nCS by the solution casting

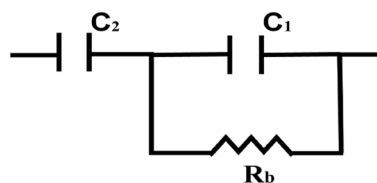


Fig. 14 Circuit model used to represent the electrical properties of blend nanocomposite

method using water as the green solvent. The formation of the blend and its nanocomposites were evident from FTIR and XRD results. Variation in d spacing and crystallinity index was a direct outcome of the efficient incorporation of nCS in PVA/CG matrix. SEM images have clearly shown the morphological changes after the addition of nCS. The smooth and homogeneous surface of PVA/CG gradually

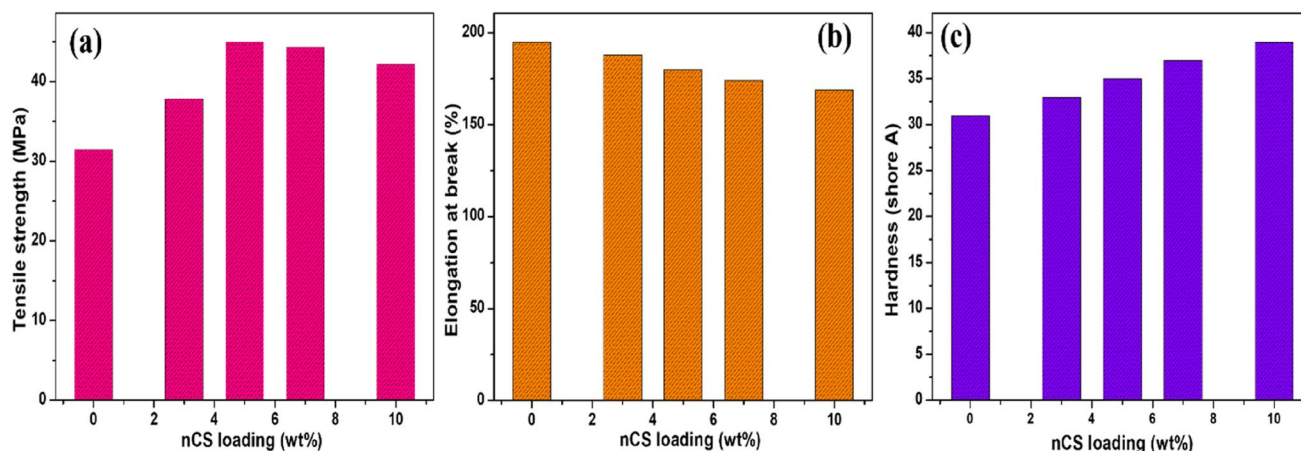


Fig. 15 Mechanical properties: **a** tensile strength **b** Elongation at break **c** Hardness of PVA/CG and nCS loaded PVA/CG

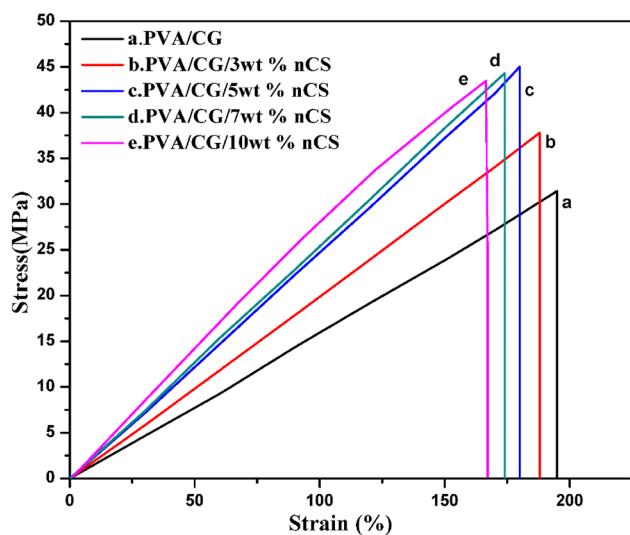


Fig. 16 Stress–strain curve of PVA/CG and PVA/CG with 0, 3, 5, 7 and 10 wt% nCS

turned rough with an increase in nCS content. The thermal properties of prepared polymer nanocomposites were also evaluated using TGA-DTG and DSC. The degradation temperature of the blend increases with the addition of nCS. The higher percentage of final char residue obtained for nanocomposites than for pure blend suggests their enhanced thermal stability. The increase in T_g and T_m upon nCS addition indicates the rigidity of the biopolymer blend with the addition of nanofiller. Investigation of electrical properties is mandatory to explore the use of these biofriendly materials in electronic applications. The AC conductivity and dielectric constant of prepared nanocomposite films were higher than those of the pure blend. Both AC conductivity and dielectric constant were highest for PVA/CG with 7 wt% nCS. The prepared

films fit best with the Arrhenius equation and activation energy for conduction was deduced from Arrhenius plots. Electric modulus and impedance analysis of pure blend and 7 wt% nCS incorporated PVA/CG were analysed at various temperatures. Mechanical aspects of films need to be considered for their applications in various fields. The tensile strength and hardness of the nanocomposite films were observed to improve, whereas the elongation at break decreased. For electrical and electrochemical devices that work at high temperatures, thermal stability and mechanical strength of material is also a matter of concern. Here we have successfully tuned the thermal, mechanical, electrical and dielectric properties of PVA/CG blend with a small amount of nCS. The prepared films can be used as components for various electronic device fabrications including sensors, transistors, dielectric layers, circuit boards, nanodielectrics, energy storage devices, actuators as they are easy to transform into desired shape, size and design. As the term sustainability has gained wide acceptance, the prepared biopolymer blend nanocomposite films are preferable to explore the field of next-generation ‘green’ electronic devices.

Author Contributions All authors contributed to the conception and design of the study. KM contributed to the material preparation, analysis and writing of the manuscript, KA performed material preparation, data collection, while MTR contributed to the conception, resources, validation, writing, review and editing.

Funding The author (K. Meera) gratefully acknowledges the financial support provided by University Grants Commission (UGC), India to carry out this research work.

Declarations

Conflict of interest The authors declare that they have no conflicts of interest.

References

- El Gohary HG, Qahtan TF, Alharbi HG, Asnag GM, Waly AL (2023) Studies of the structural, optical, thermal, electrical and dielectric properties of a polyvinyl alcohol/Sodium alginate blend doped with Cu nanoparticles and ZnO nanorods as hybrid nanofillers for use in energy storage devices. *J Polym Environ*. <https://doi.org/10.1007/s10924-023-02785-2>
- Gasti T, Hiremani VD, Kesti SS, Vanjeri VN, Goudar N, Masti SP, Thimmappa SC, Chougale RB (2021) Physicochemical and antibacterial evaluation of poly (vinyl alcohol)/guar gum/silver nanocomposite films for food packaging applications. *J Polym Environ* 29:3347–3363. <https://doi.org/10.1007/s10924-021-02123-4>
- Hajji S, Ktari N, Ben SR, Boufi S, Debeaufort F, Nasri M (2022) Development of nanocomposite films based on chitosan and gelatin loaded with chitosan-tripolyphosphate nanoparticles: antioxidant potentials and applications in wound healing. *J Polym Environ* 30:833–854. <https://doi.org/10.1007/s10924-021-02239-7>
- Chomachayi MD, Jalali-arani A, Urreaga JM (2021) A comparison of the effect of silk fibroin nanoparticles and microfibers on the reprocessing and biodegradability of PLA/PCL blends. *J Polym Environ* 29:2585–2597. <https://doi.org/10.1007/s10924-021-02053-1>
- Meera K, Ramesan MT (2023) Development of high-performance biopolymer nanocomposites derived from carboxymethyl chitosan/boehmite via green synthesis. *Polym Compos* 44:1135–1148. <https://doi.org/10.1002/pc.27159>
- Abdullah OG, Hanna RR, Ahmed HT, Mohamad AH, Saleem SA, Saeed MA (2021) Conductivity and dielectric properties of lithium-ion biopolymer blend electrolyte-based film. *Results Phys* 24:104135. <https://doi.org/10.1016/j.rinp.2021.104135>
- Hu W, Zou Z, Li H, Zhang Z, Yu J, Tang Q (2022) Fabrication of highly transparent and multifunctional polyvinyl alcohol/starch-based nanocomposite films using zinc oxide nanoparticles as compatibilizers. *Int J Biol Macromol* 204:284–292. <https://doi.org/10.1016/j.ijbiomac.2022.02.020>
- Suvarna S, Furhan RMT (2023) Structural, conductivity, mechanical and wettability properties of copper alumina reinforced chlorinated polyethylene/polyvinyl chloride blend nanocomposites. *Res Chem Intermed* 49:1891–1908. <https://doi.org/10.1007/s11164-022-04881-9>
- Abdulwahid RT, Aziz BS, Kadir MF (2022) Design of proton conducting solid biopolymer blend electrolytes based on chitosan-potato starch biopolymers: deep approaches to structural and ion relaxation dynamics of H⁺ ion. *J Appl Polym Sci* 139:e52892. <https://doi.org/10.1002/app.52892>
- Abdulwahid RT, Aziz SB, Kadir MF (2022) Insights into ion transport in biodegradable solid polymer blend electrolyte based on FTIR analysis and circuit design. *J Phys Chem Solids* 167:110774. <https://doi.org/10.1016/j.jpcs.2022.110774>
- Swapna VP, Krishnan M, Abhisha VS, Stephen R (2021) Efficient cage structured polyhedral oligomeric silsesquioxane embedded poly(vinyl alcohol) membranes: Thermal degradation and mechanical stability in hydrated condition. *J Appl Polym Sci* 138:e51377. <https://doi.org/10.1002/app.51377>
- Meera K, Ramesan MT (2023) Performance of boehmite nanoparticles reinforced carboxymethyl chitosan/polyvinyl alcohol blend nanocomposites tailored through green synthesis. *J Polym Environ* 31:447–460. <https://doi.org/10.1007/s10924-022-02649-1>
- Abdullah ZW, Dong Y, Davies IJ, Barbhuiya S (2017) PVA, PVA blends, and their nanocomposites for biodegradable packaging application. *Polym Plast Technol Eng* 56:1307–1344. <https://doi.org/10.1080/03602559.2016.1275684>
- Xu J, Jiang XS, Peng L, Wang Y, Shang S, Miao D, Guo R (2019) AgNps-PVA-coated woven cotton fabric: preparation, water repellency, shielding properties and antibacterial activity. *J Ind Text* 48:1545–1565. <https://doi.org/10.1177/1528083718764908>
- Porto BC, Augusto PED, Cristianini M (2015) Comparative study between technological Properties of cashew tree gum and Arabic gum. *J Polym Environ* 23:392–399. <https://doi.org/10.1007/s10924-014-0698-z>
- de Azevedo GA, Heinrichs MC, Moraes ÂM (2022) Cashew tree gum for biomaterials engineering: a versatile raw material in consolidation. *J Appl Polym Sci* 139:e52484. <https://doi.org/10.1002/app.52484>
- Mochane MJ, Sefadi JS, Motsoeneng TS, Mokoena TE, Mofokeng TG, Mokheba TC (2020) The effect of filler localization on the properties of biopolymer blends, recent advances: a review. *Polym Compos* 41:2958–2979. <https://doi.org/10.1002/pc.25590>
- Ramesan MT, Subburaj M, Mathew G, Bahuleyan BK (2023) Utilization of copper sulphide nanoparticles for the development of cashew tree gum/ chitin biopolymer blend nanocomposites. *J Thermoplast Compos Mater* 36:984–1003. <https://doi.org/10.1177/08927057211046282>
- Migdadi AB, Ahmad AA, Alsaad AM, Telfah A (2022) Synthesis, optoelectronic and thermal characterization of PMMA-MWCNTs nanocomposite thin films incorporated by ZrO₂ NPs. *J Mater Sci Mater Electron* 33:5087–5104. <https://doi.org/10.1007/s10854-022-07699-8>
- Hidangmayum A, Dwivedi P (2022) Chitosan based nanoformulation for sustainable agriculture with special Reference to abiotic stress: a review. *J Polym Environ* 30:1264–1283. <https://doi.org/10.1007/s10924-021-02296-y>
- Hamedi H, Moradi S, Hudson SM, Tonelli AE, King MW (2022) Chitosan based bio-adhesives for biomedical applications: a review. *Carbohydr Polym* 282:119100. <https://doi.org/10.1016/j.carbpol.2022.119100>
- Begum ERA, Rajaiah S, Bhavani K, Devi M, Karthika K, Priya CG (2017) Evaluation of extracted chitosan from portunus pelagicus for the preparation of chitosan alginate blend scaffolds. *J Polym Environ* 25:578–585. <https://doi.org/10.1007/s10924-016-0834-z>
- Selim SE, Meligi GA, Abdelhamid AE, Mabrouk MA, Husain AI (2022) Novel composite films based on acrylic fibers waste/nano-chitosan for congo red adsorption. *J Polym Environ* 30:2642–2657. <https://doi.org/10.1007/s10924-022-02378-5>
- Cazón P, Vázquez M, Velázquez G (2018) Novel composite films based on cellulose reinforced with chitosan and polyvinyl alcohol: Effect on mechanical properties and water vapour permeability. *Polym Test* 69:536–544. <https://doi.org/10.1016/j.polymertesting.2018.06.016>
- Srinivasa P, Ramesh M, Kumar K, Tharanathan R (2003) Properties and sorption studies of chitosan-polyvinyl alcohol blend films. *Carbohydr Polym* 53:431–438. [https://doi.org/10.1016/S0144-8617\(03\)00105-X](https://doi.org/10.1016/S0144-8617(03)00105-X)
- Shyly PM, Sridevi NA, Premkumar PS (2022) Thermal and mechanical studies of nanochitosan incorporated polymethyl methacrylate-based composite electrolytes. *J Eng Appl Sci* 69:26. <https://doi.org/10.1186/s44147-022-00077-5>
- Moreira BR, Pereira-Junior MA, Fernandes KF, Batista KA (2020) An ecofriendly edible coating using cashew gum polysaccharide and polyvinyl alcohol. *Food Biosci* 37:100722. <https://doi.org/10.1016/j.fbio.2020.100722>
- Wang X, Hu Y, Zhang Z, Zhang B (2022) The application of thymol-loaded chitosan nanoparticles to control the biodegradation of cultural heritage sites. *J Cult Herit* 53:206–211. <https://doi.org/10.1016/j.culher.2021.12.002>
- Martins CS, Morgado DL, Assis OB (2016) Cashew gum-chitosan blended films: spectral, mechanical and surface. *Macromol Res* 24:691–697. <https://doi.org/10.1007/s13233-016-4103-8>

30. Ricciardi R, Auriemma F, De Rosa C, Lauprêtre F (2004) X-ray diffraction analysis of poly (vinyl alcohol) hydrogels, obtained by freezing and thawing techniques. *Macromolecules* 37:1921–1927. <https://doi.org/10.1021/ma035663q>
31. Olorunsola EO, Bhatia PG, Tytler BA, Adikwu MU (2016) Thermochemical properties of hydrophilic polymers from cashew and khaya exudates and their implications on drug delivery. *J Drug Deliv*. <https://doi.org/10.1155/2016/7496585>
32. Shetta A, Kegere J, Mamdouh W (2019) Comparative study of encapsulated peppermint and green tea essential oils in chitosan nanoparticles: encapsulation, thermal stability, in-vitro release, antioxidant and antibacterial activities. *Int J Biol Macromol* 126:731–742. <https://doi.org/10.1016/j.ijbiomac.2018.12.161>
33. Ramesan MT, Jose C, Jayakrishnan P, Anilkumar T (2018) Multifunctional ternary composites of poly (vinyl alcohol)/cashew tree gum/pumice particles. *Polym Compos* 39:38–45. <https://doi.org/10.1002/pc.23899>
34. Al-Muntaser AA, Pashameah RA, Saeed A, Alwafi R, Alzahrani E, AlSubhi SA, Yassin AY (2023) Boosting the optical, structural, electrical, and dielectric properties of polystyrene using a hybrid GNP/Cu nanofiller: novel nanocomposites for energy storage applications. *J Mater Sci Mater Electron* 34:678. <https://doi.org/10.1007/s10854-023-10104-7>
35. Terzioğlu P, Güney F, Parın FN, Şen İ, Tuna S (2021) Biowaste orange peel incorporated chitosan/polyvinyl alcohol composite films for food packaging applications. *Food Package Shelf Life* 30:100742. <https://doi.org/10.1016/j.fpsl.2021.100742>
36. Soliman TS, Vshnikov SA (2019) Effect of Fe nanoparticles on the structure and optical properties of polyvinyl alcohol nanocomposite films. *J Non-Cryst Solids* 519:119452. <https://doi.org/10.1016/j.jnoncrysol.2019.05.028>
37. Moghadam A, Mobarakeh MS, Safaei M, Kariminia S (2021) Synthesis and characterization of novel bio-nanocomposite of polyvinyl alcohol-Arabic gum-magnesium oxide via direct blending method. *Carbohydr Polym* 260:117802. <https://doi.org/10.1016/j.carbpol.2021.117802>
38. Khalili H, Hamid Salim M, Tlemcani S, Makhlof R, Hassani FZ, Ablouh H, Kassab Z, El Achaby M (2022) Bio-nanocomposite films based on cellulose nanocrystals filled polyvinyl alcohol/alginate polymer blend. *J Fibers Polym Compos* 1:77–96. <https://doi.org/10.55043/jfpc.v1i2.56>
39. Parvathi K, Ramesan MT (2023) Tailoring the structural, electrical and thermal properties of zinc oxide reinforced chlorinated natural rubber/poly (indole) blend nanocomposites for flexible electrochemical devices. *J Polym Res* 30:55. <https://doi.org/10.1007/s10965-022-03427-2>
40. El Miri N, Abdelouahdi K, Zahouily M, Fihri A, Barakat A, Solhy A, El Achaby M (2015) Bio-nanocomposite films based on cellulose nanocrystals filled polyvinyl alcohol/chitosan polymer blend. *J Appl Polym Sci* 132:42004. <https://doi.org/10.1002/app.42004>
41. Sankar S, Ramesan MT (2022) Thermal, optical and temperature dependent electrical properties poly(aniline-co-pyrrole)/copper alumina nanocomposites for optoelectronic devices. *J Therm Anal Calorim* 147:13375–13387. <https://doi.org/10.1007/s10973-022-11670-4>
42. Suvarna S, Niranjana VS, Subburaj M, Ramesan MT (2022) Temperature-dependent conductivity, optical properties, thermal stability and dielectric modelling studies of Cu-Al₂O₃/CPE/PVC blend nanocomposites. *Bull Mater Sci* 45:246. <https://doi.org/10.1007/s12034-022-02829-8>
43. Alghamdi HM, Abutalib MM, Rajeh A, Mannaa MA, Nur O, Abdelrazek EM (2022) Effect of the Fe₂O₃/TiO₂ nanoparticles on the structural, mechanical, electrical properties and antibacterial activity of the biodegradable chitosan/polyvinyl alcohol blend for food packaging. *J Polym Environ* 30:3865–3874. <https://doi.org/10.1007/s10924-022-02478-2>
44. Meera K, Ramesan MT (2023) Tailoring the performance of boehmite nanoparticles reinforced carboxymethyl chitosan/cashew gum blend nanocomposites via green synthesis. *Polymer* 268:125706. <https://doi.org/10.1016/j.polymer.2023.125706>
45. Alsulami QA, Rajeh A (2021) Synthesis of the SWCNTs/TiO₂ nanostructure and its effect study on the thermal, optical, and conductivity properties of the CMC/PEO blend. *Results Phys* 28:104675. <https://doi.org/10.1016/j.rinp.2021.104675>
46. Rajeswari N, Selvasekarapandian S, Sanjeeviraja C, Kawamura J, Asath Bahadur S (2014) A study on polymer blend electrolyte based on PVA/PVP with proton salt. *Polym Bull* 71:1061–1080. <https://doi.org/10.1007/s00289-014-1111-8>
47. Abdelrazek EM, Abdelghany AM, Tarabiah AE, Zidan HM (2019) AC conductivity and dielectric characteristics of PVA/PVP nanocomposite filled with MWCNTs. *J Mater Sci Mater Electron* 30:15521–15533. <https://doi.org/10.1007/s10854-019-01929-2>
48. Rajesh K, Crasta V, Rithin Kumar NB, Shetty G, Rekha PD (2019) Structural, optical, mechanical and dielectric properties of titanium dioxide doped PVA/PVP nanocomposite. *J Polym Res* 26:99. <https://doi.org/10.1007/s10965-019-1762-0>
49. Yassin AY (2020) Dielectric spectroscopy characterization of relaxation in composite based on (PVA–PVP) blend for nickel–cadmium batteries. *J Mater Sci Mater Electron* 31:19447–19463. <https://doi.org/10.1007/s10854-020-04478-1>
50. Alharbi EM, Rajeh A (2022) Tailoring the structural, optical, dielectric, and electrical properties of PEO/PVA blend using graphene nanoplates for energy storage devices. *J Mater Sci Mater Electron* 33:22196–22207
51. Parvathi K, Ramesan MT (2023) Effect of titanium dioxide on the structural, thermal and electrical properties of chlorinated natural rubber/poly (indole) blend nanocomposites for flexible nanoelectronics devices. *J Appl Polym Sci* 140:e53621. <https://doi.org/10.1002/app.53621>
52. Yassin AY, Abdelghany AM (2021) Synthesis and thermal stability, electrical conductivity and dielectric spectroscopic studies of poly (ethylene-co-vinyl alcohol)/graphene oxide nanocomposite. *Phys B Condens Matter* 608:412730. <https://doi.org/10.1016/j.physb.2020.412730>
53. Gami F, Algethami N, Ragab HM, Tarabiah AE (2022) Structural, optical and electrical studies of chitosan/polyacrylamide blend filled with synthesized selenium nanoparticles. *J Mol Struct* 1257:132631. <https://doi.org/10.1016/j.molstruc.2022.132631>
54. Furhan SS, Ramesan MT (2022) Optical and electrical properties of copper alumina nanoparticles reinforced chlorinated polyethylene composites for optoelectronic devices. *J Indian Chem Soc* 99:100772. <https://doi.org/10.1016/j.jics.2022.100772>
55. Marf AS, Abdullah RM, Aziz SB (2020) Structural, morphological, electrical and electrochemical properties of PVA: CS-based proton-conducting polymer blend electrolytes. *Membranes* 10:71. <https://doi.org/10.3390/membranes10040071>
56. Mobarak NN, Ahmad A, Abdullah MP, Ramli N, Rahman MY (2013) Conductivity enhancement via chemical modification of chitosan based green polymer electrolyte. *Electrochim Acta* 92:161–167. <https://doi.org/10.1016/j.electacta.2012.12.126>
57. Takkalkar P, Griffin G, Kao N (2019) Enhanced mechanical and barrier performance of poly (Lactic Acid) based nanocomposites using surface acetylated starch nanocrystals. *J Polym Environ* 27:2078–2088. <https://doi.org/10.1007/s10924-019-01484-1>
58. Pereira R, Tojeira A, Vaz DC, Mendes A, Bártolo P (2011) Preparation and characterization of films based on alginate and aloe vera. *Int J Polym Anal Charact* 16:449–464. <https://doi.org/10.1080/1023666X.2011.599923>
59. Suvarna S, Furhan PK, Ramesan MT (2023) Role of copper alumina nanoparticles on the performance of polyvinylchloride

- nanocomposites. *J Vinyl Addt Technol* 29:17–28. <https://doi.org/10.1002/vnl.21939>
60. Rajabinejad H, Zoccola M, Patrucco A, Montarsolo A, Chen Y, Ferri A, Muresan A, Tonin C (2020) Fabrication and properties of keratose/polyvinyl alcohol blend films. *Polym Bull* 77:3033–3046. <https://doi.org/10.1007/s00289-019-02889-7>

Springer Nature or its licensor (e.g. a society or other partner) holds exclusive rights to this article under a publishing agreement with the author(s) or other rightsholder(s); author self-archiving of the accepted manuscript version of this article is solely governed by the terms of such publishing agreement and applicable law.

Publisher's Note Springer Nature remains neutral with regard to jurisdictional claims in published maps and institutional affiliations.